

# General solution to inhomogeneous dephasing and smooth pulse dynamical decoupling

Junkai Zeng, Xiu-Hao Deng, and Edwin Barnes\*

*Department of Physics, Virginia Tech, Blacksburg, Virginia 24061, USA*

In order to achieve the high-fidelity quantum control needed for a broad range of quantum information technologies, reducing the effects of noise and system inhomogeneities is an essential task. It is well known that a system can be decoupled from noise or made insensitive to inhomogeneous dephasing dynamically by using carefully designed pulse sequences based on square or delta-function waveforms such as Hahn spin echo or CPMG. However, such ideal pulses are often challenging to implement experimentally with high fidelity. Here, we uncover a geometrical framework that allows one to visualize all possible driving fields that dynamically correct for errors in the evolution of a qubit. Our approach enables one to generate an unlimited number of smooth, experimentally feasible pulses that perform dynamical decoupling or dynamically corrected gates to arbitrarily high order. We demonstrate that this scheme can significantly enhance the fidelity of single-qubit operations in systems with slowly fluctuating noise.

In recent years, the prospect of enhanced technologies that exploit the principles of quantum mechanics has attracted great interest from many fields in physics and beyond. These efforts are geared toward several envisioned applications, including information processing [1–5], secure communications [6, 7], and sensing [8–10], and enormous progress has been made in engineering and optimizing coherent quantum systems for these purposes. However, decoherence caused by the environment or other factors continues to be a primary impediment to realizing quantum technologies [11–14]; overcoming this challenge requires improvements not only in system engineering [15–17], but also in how such systems are controlled.

It has been known since the early days of nuclear magnetic resonance that it is possible to design driving fields that suppress adverse effects caused by fluctuations in the system Hamiltonian or in the driving field itself. The simplest example is the Hahn spin echo [18], in which a fast ( $\delta$ -function)  $\pi$ -pulse is applied halfway through the evolution of a precessing spin, guaranteeing that the spin returns to its initial state at the end of the evolution regardless of the precession rate. This has long been a standard technique to combat inhomogeneous dephasing—the loss of coherence due to variations in precession frequency in spin ensembles. Spin echo and related multi-pulse sequences [19–26] have also been widely employed to mitigate other types of decoherence such as environmental noise fluctuations [27–29]. Much work has been done to extend dynamical decoupling to not only preserve the state of the system, but to also cancel errors while performing operations on the system (dynamical gate correction) [30–39].

Although these dynamical decoupling methods have been broadly successful, there are many systems, especially in the context of quantum information technologies, where they exhibit substantial drawbacks. This is because the highly idealized pulse waveforms needed, i.e.,  $\delta$ -functions or square pulses, can be challenging to gen-

erate in systems where the dynamics occurs on nanosecond timescales, pushing the limits of current waveform generators. This, combined with the need to perform operations with an unprecedented level of accuracy, makes standard dynamical decoupling methods inadequate in many systems. In addition, building control sequences from a very restricted set of pulse shapes leaves few tunable parameters and leads to unnecessarily long sequences that may compete with other decoherence or loss mechanisms that become important on longer timescales.

In this paper, we develop a systematic method to generate arbitrarily many smooth driving fields that implement dynamical decoupling and dynamically corrected gates for a resonantly driven qubit. In fact, we obtain the entire solution space of driving fields that combat inhomogeneous dephasing and environmental noise fluctuations in the qubit energy splitting. We do this by developing a geometrical framework in which the qubit evolution is mapped onto a curve lying within a two-dimensional plane, where the curvature of the curve determines the shape of the driving pulse, and the length of the curve equals the pulse duration. We show that any closed curve corresponds to an evolution in which the leading-order error vanishes, while any closed curve with zero net area yields a driving field that cancels up to second-order errors. Higher-order error cancellations also admit geometrical interpretations within this construction. We give explicit examples of smooth pulses that perform dynamical decoupling or dynamically corrected gates to arbitrarily high order. We also demonstrate the effectiveness of our solutions in the presence of time-dependent  $1/f$  noise.

We focus on the case of a driven qubit described by the following Hamiltonian:

$$\mathcal{H}(t) = \frac{\Omega(t)}{2} \sigma_z + \delta\beta \sigma_x. \quad (1)$$

Here,  $\Omega(t)$  is the control field, while  $\delta\beta$  is an unknown stochastic fluctuation.  $\mathcal{H}(t)$  is one of the most widely used models of decoherence due to slow noise [40–42]. We can view it as describing a qubit with a tunable energy splitting given by  $\Omega(t)$ , with  $\delta\beta$  interpreted as a

---

\* efbarnes@vt.edu

fluctuating transverse field. Alternatively, we can think of  $\Omega(t)$  as the amplitude of a resonant, monochromatic driving field, in which case  $\delta\beta$  represents a fluctuation in the detuning caused by fluctuations in the qubit energy splitting which give rise to inhomogeneous dephasing. In the second case,  $\mathcal{H}(t)$  is the Hamiltonian in a frame which rotates with the driving field (in the rotating wave approximation) and which is rotated by  $\pi/2$  relative to the qubit quantization axis.

We parametrize the evolution operator according to

$$U(t) = \begin{pmatrix} u_1(t) & -u_2^*(t) \\ u_2(t) & u_1^*(t) \end{pmatrix}. \quad (2)$$

It is notoriously difficult to solve the Schrödinger equation,  $i\dot{U}(t) = \mathcal{H}(t)U(t)$ , to obtain  $u_1$  and  $u_2$  analytically aside from a few special choices of  $\Omega(t)$ . These special choices include the cases of  $\delta$ -function pulses and square pulses, which is the primary reason why most dynamical decoupling sequences are based on these ideal waveforms. There exist methods for solving this equation more generally using a type of reverse-engineering [38, 43, 44], but these techniques do not apply for the form of  $\mathcal{H}(t)$  we are considering here. Although we cannot obtain closed-form solutions in general, we can obtain solutions as a power series in  $\delta\beta$  [35]:

$$\begin{aligned} u_1(t) &= e^{-i\phi(t)/2}(g_0(t) - g_2(t)\delta\beta^2 + g_4(t)\delta\beta^4 - \dots), \\ u_2(t) &= -ie^{i\phi(t)/2}(g_1^*(t)\delta\beta - g_3^*(t)\delta\beta^3 + \dots), \end{aligned} \quad (3)$$

where  $\phi(t) = \int_0^t \Omega(\tau)d\tau$  is the qubit rotation angle, and the coefficients of  $\delta\beta$  obey a recurrence relation:

$$g_n(t) = \int_0^t e^{i\phi(\tau)} g_{n-1}^*(\tau) d\tau, \quad (4)$$

with  $g_0(t) = 1$ . To obtain robust quantum operations with operation time  $T$ , we must find functions  $\phi(t)$  (from which we obtain the driving field via  $\Omega(t) = \dot{\phi}$ ) which yield vanishing error coefficients,  $g_m(T) = 0$ , for all  $m \leq n$ , where  $n$  is the desired degree of robustness. Since  $g_m$  is complex, this gives two real constraints on  $\Omega(t)$  for each odd  $m$ . For even  $m$ , there is only one real constraint because unitarity requires  $|u_1|^2 + |u_2|^2 = 1$ , which from Eq. (3) implies that at any time  $t$ ,

$$\text{Re}[g_n] = \sum_{k=1}^{n/2-1} (-1)^{k-1} \text{Re}[g_k g_{n-k}^*] - \frac{(-1)^{n/2}}{2} |g_{n/2}|^2. \quad (5)$$

Thus for even  $n$ ,  $\text{Re}[g_n(T)] = 0$  is automatically satisfied if  $g_m(T) = 0$  for all  $m \leq n/2$ , and we are left with one real independent constraint at this order:  $\text{Im}[g_n(T)] = 0$ . For a sequence of  $\delta$ -function  $\pi$  pulses,  $e^{i\phi(\tau)} = \pm 1$  is the associated characteristic function [40], and it is easy to show that  $g_n(T) = 0$  for spin echo, CPMG, and other well known sequences. In what follows, we will show that there exists a geometrical framework that allows us to find all possible driving fields that satisfy these constraints order by order.

We begin by considering the first-order constraint,  $g_1(T) = 0$ . The solution space of this constraint can be constructed by first parametrizing this function in terms of plane Cartesian coordinates:

$$g_1(t) = x(t) + iy(t). \quad (6)$$

Since the time derivative of  $g_1(t)$  is a pure phase [Eq. (4)], we find the following restriction between  $x(t)$  and  $y(t)$ :

$$\dot{x}^2 + \dot{y}^2 = 1. \quad (7)$$

The error coefficient,  $g_1(t)$ , can thus be viewed as a curve in the plane spanned by  $x$  and  $y$  which starts at the origin at time  $t = 0$ :  $x(0) = y(0) = 0$ , and with slope  $\dot{x}^2(0) + \dot{y}^2(0) = 1$ . There is a one-to-one correspondence between these plane curves and possible driving fields which follows from the relation between  $g_1$  and the rotation angle  $\phi$ :

$$\Omega(t) = \dot{x}\ddot{y} - \dot{y}\ddot{x} = \frac{\dot{x}\ddot{y} - \dot{y}\ddot{x}}{(\dot{x}^2 + \dot{y}^2)^{3/2}}. \quad (8)$$

The above formula for  $\Omega(t)$  has a surprisingly simple geometric interpretation: it is precisely equal to the signed curvature,  $\kappa$ , of the plane curve, which is defined to be the proportionality coefficient between the derivative of the curve's tangent vector and its normal vector:  $\dot{\mathbf{V}}(t) = \kappa(t)\mathbf{N}(t)$ . Since the curvature is defined independently of parametrization, we may express it in terms of a general parameter  $\lambda$  along the curve:

$$\kappa(\lambda) = \frac{x'y'' - y'x''}{(x'^2 + y'^2)^{3/2}}, \quad (9)$$

where the prime denotes differentiation with respect to  $\lambda$ . We are thus free to use any parametrization we choose to define the plane curve. Once we have made this choice, we can extract the driving field:  $\Omega(t) = \kappa(\lambda(t))$ , where the mapping between  $\lambda$  and  $t$  is determined from Eq. (7):

$$t = \int_0^\lambda d\mu \sqrt{[x'(\mu)]^2 + [y'(\mu)]^2}. \quad (10)$$

Notice that the integral on the right hand side measures distance along the curve, meaning that time  $t$  can be thought of as the arc-length parametrization of the curve. The driving field is thus the curvature of the plane curve expressed as a function of arc length. This also means that the evolution time  $T$  is equal to the total length of the curve. Also notice that the curvature, and hence the driving field, remain invariant under rigid rotations and translations of the curve.

Requiring the first-order error to vanish at  $t=T$  is equivalent to imposing the simple condition that the curve is closed:  $x(\Lambda) = y(\Lambda) = 0$ , where  $\Lambda \equiv \lambda(T)$ . Also, the net rotation angle,  $\phi(T)$ , is determined by the angle,  $\Delta\theta$ , subtended by the curve at the origin:

$$\phi(T) = \int_0^T dt \Omega(t) = \arctan\left(\frac{y'}{x'}\right)\Bigg|_0^\Lambda = \Delta\theta + \pi. \quad (11)$$

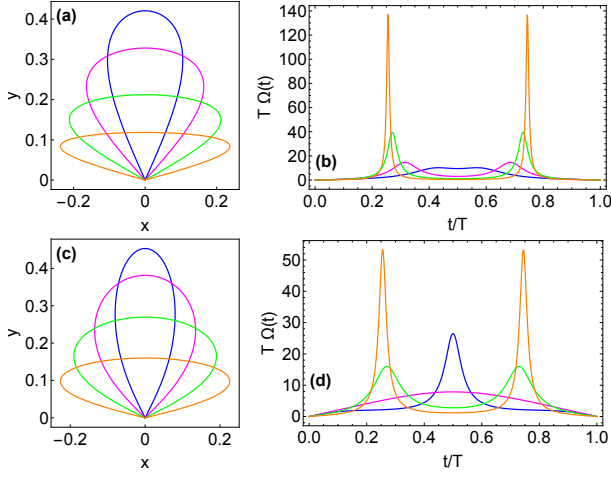


FIG. 1. Pulses which cancel the first-order error. (a) Modified Geroni half-lemniscates, Eq. (12), and (c) modified Bernoulli half-lemniscates, Eq. (13), with opening angles  $\Delta\theta = \pi - 2\text{arccot}(\alpha)$  for  $\alpha = 0.5, 1, 2, 4$ . All curves have been rescaled to have unit length. (b,d) Corresponding pulses that implement  $z$  rotations with angle  $\phi(T) = \Delta\theta + \pi$ .

This formula is valid modulo  $2\pi$  because of the multi-valued nature of the inverse tangent. Here, it is important to emphasize that *any* closed curve that starts and ends at the origin and which subtends the same angle,  $\Delta\theta$ , at the origin yields a pulse that implements the same qubit rotation while canceling the leading-order error. Conversely, any pulse which accomplishes these tasks corresponds to a plane curve of this form. (Note that in this framework, a single spin echo pulse is represented by the limiting case in which the closed curve collapses on itself to form a straight line segment extending away from the origin a finite distance  $r$ ; the  $\delta$ -function  $\pi$  pulse corresponds to the sharp turning point at  $r$ . More general  $\delta$ -function pulse sequences also correspond to collapsed line segments, with one turning point per pulse.) This geometrical interpretation not only makes it easy to visualize the complete solution space of the first-order constraint, it also makes it easy to systematically determine optimal pulses for a given rotation. This is because the driving field is proportional to the curvature, providing a simple way to visualize and to impose constraints on the smoothness of the pulse. In addition, the fact that the evolution time is equal to the length of the curve allows for optimization of the operation time given smoothness constraints.

We can construct simple, explicit examples of smooth pulses which cancel the first-order error by modifying the well known lemniscates (figure-eight curves) of Geroni:

$$x(\lambda) = (\alpha/2) \sin(2\lambda), \quad y(\lambda) = \sin \lambda, \quad (12)$$

and of Bernoulli:

$$x(\lambda) = \frac{\alpha \sin(2\lambda)}{3 + \cos(2\lambda)}, \quad y(\lambda) = \frac{2 \sin \lambda}{3 + \cos(2\lambda)}. \quad (13)$$

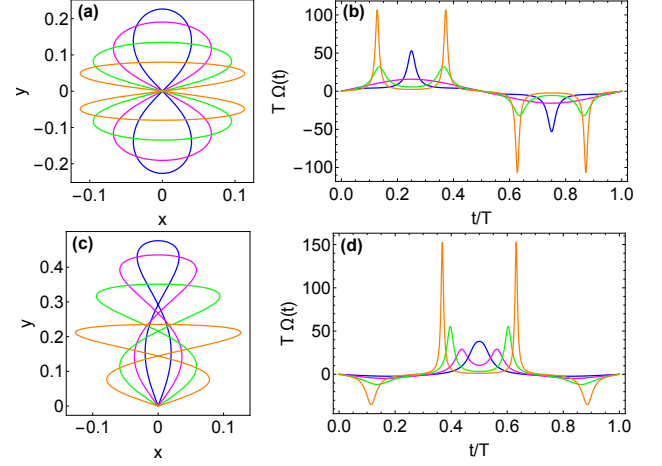


FIG. 2. Pulses which cancel error to second order. (a) Modified Bernoulli lemniscates, Eq. (13), for  $\alpha = 0.5, 1, 2, 4$ . All curves have been rescaled to have unit length. (b) Four different pulses corresponding to plane curves in (a) that implement dynamical decoupling ( $\phi(T) = 0$ ). (c) Zero-area curves from Eq. (15) with  $a = 1/4, 1/2, 1, 2$  and  $b = -6a$ . (d) Pulses corresponding to curves in (c) that perform different rotations with angle determined by Eq. (16).

In both cases, we choose the maximal value of  $\lambda$  to be  $\Lambda = \pi$  in order to retain only half the lemniscate, giving a closed curve that subtends an angle  $\Delta\theta < \pi$  at the origin. We have included the free parameter  $\alpha$  in order to make this angle, and hence the rotation angle  $\phi(T)$ , adjustable:  $\Delta\theta = \pi - 2\text{arccot}(\alpha)$ . Fig. 1 shows the resulting half-lemniscates and the corresponding pulses (obtained from the curvature, Eq. (9)) for both the Geroni and Bernoulli curves. Together, these solutions give, for each choice of rotation angle  $\phi(T)$ , two different pulses which implement the same rotation while canceling the leading-order error. Of course, infinitely many smooth pulses which achieve the same task can be generated from curves qualitatively similar to those shown in Fig. 1(a),(c). Notice that if we keep the pulse time fixed, then implementing larger rotation angles requires sharper peaks in the pulse, a fact which is clear from the geometrical construction since the plane curve is forced to have sharper bends as  $\Delta\theta$  increases.

Because of the recursive nature of the error constraints evident in Eq. (4), requiring higher-order errors to cancel can be interpreted as imposing additional constraints on the shape of the plane curve. Consider the second-order constraint,  $g_2(T) = 0$ . From Eq. (5) we know that  $\text{Re}[g_2(T)] = 0$  if the first-order error vanishes,  $g_1(T) = 0$ , i.e., if the plane curve is closed. The remaining second-order error can be written as

$$\text{Im}[g_2(T)] = \int_0^\Lambda d\lambda [x'(\lambda)y(\lambda) - y'(\lambda)x(\lambda)]. \quad (14)$$

Remarkably, this integral is exactly twice the area enclosed by the plane curve, meaning that the second-order

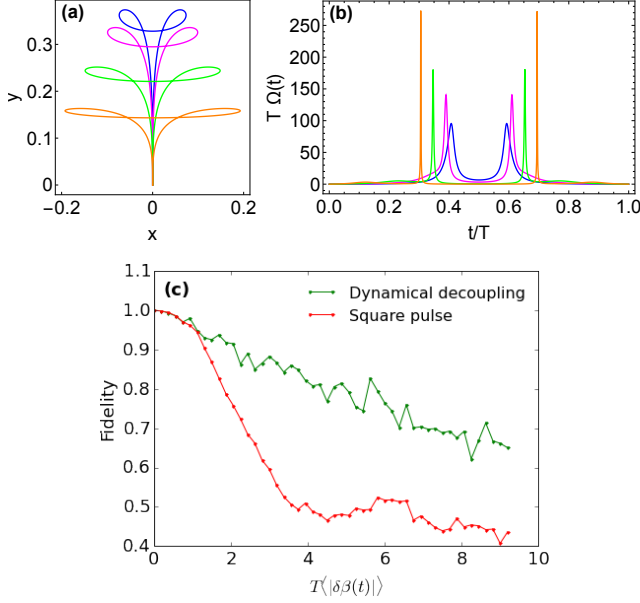


FIG. 3. (a) Plane curves from Eq. (15) with  $a = 2/3, 1, 2, 4$  and  $b = -a$ . (b) Corresponding pulses, all of which implement  $3\pi$  rotations while canceling up to second-order errors. (c) Fidelity versus time-averaged noise strength of  $1/f$  noise for  $3\pi$  pulse with  $a = 2/3$  compared with square pulse that implements the same rotation with the same duration  $T$ .

error vanishes if and only if the net area enclosed by the curve is zero. Thus we find that pulses which cancel both first- and second-order errors are in one-to-one correspondence with closed plane curves that enclose a vanishing net area. Full lemniscates such as those of Geroni and Bernoulli, Eqs. (12), (13), satisfy these requirements, provided we now take  $\Lambda = 2\pi$ . The resulting curves and corresponding pulses are shown in Fig. 2(a),(b). An important difference compared to the first-order case is that now, each of these pulses implements dynamical decoupling, i.e., an identity operation with  $\phi(T) = 0$ . This is because the angle subtended by the initial and final legs of the plane curves is equal to  $\pi$  regardless of the value of  $\alpha$ . We see from the figure that it is easy to obtain arbitrarily many smooth pulses that perform dynamical decoupling up to second order.

In order to perform nontrivial rotations while canceling errors up to second order, we need to consider more general zero-area curves that exhibit a kink at the origin. We introduce one family of such curves, parametrized as

$$\begin{aligned} x(\lambda) &= [a + b \cos(\lambda)] \sin(\lambda), \\ y(\lambda) &= \lambda(2\pi - \lambda) + (4 + b/a)[\cos(\lambda) - 1], \end{aligned} \quad (15)$$

with  $\Lambda = 2\pi$ , and where the rotation angle is given by

$$\phi(T) = 2 \arctan\left(\frac{a+b}{2\pi}\right) + \pi. \quad (16)$$

Restricting attention to pulses that start and end at zero,  $\Omega(0) = \Omega(T) = 0$ , requires the parameters  $a$  and  $b$  to be

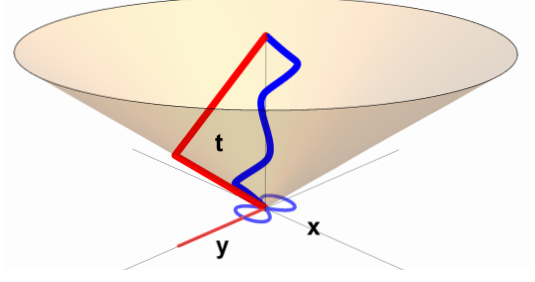


FIG. 4. There is a one-to-one correspondence between driving fields and lightlike (null) curves in 3D Minkowski space. Driving fields which cancel the first-order error correspond to lightlike curves that start and end at the origin. The 2D plane curves are the projections of these lightlike curves onto the  $xy$  plane. The blue line is the lightlike curve for the Bernoulli lemniscate, Eq. (13), with  $\alpha = 2$ . The red line is the lightlike curve corresponding to a spin echo pulse (a  $\delta$ -function  $\pi$ -pulse applied halfway through the evolution). The 2D projections of both lightlike curves are also shown. The lightlike curves must lie within the lightcone with apex at  $x = y = t = 0$ .

related through either  $b = -a$  or  $b = -6a$ . The former condition produces  $3\pi$  rotations while the latter allows for a wide range of rotation angles. Examples of curves with  $b = -6a$  and their corresponding pulses are shown in Fig. 2(c),(d). Fig. 3 shows examples of curves with  $b = -a$ . Since our cancellation constraints, Eq. (4), are derived assuming quasistatic noise in which  $\delta\beta$  is an unknown but constant variation in the Hamiltonian, it is important to consider the performance of the resulting pulses in the presence of time-dependent noise fluctuations. Perhaps the most ubiquitous type of classical time-dependent noise in the context of quantum technologies is  $1/f$  noise [11, 14, 45, 46]. Fig. 3(c) shows the operation fidelity [47] for the pulse corresponding to  $a = 2/3 = -b$  (blue curve in Fig. 3(b)) as a function of noise strength. For comparison, the figure also shows the performance of a square pulse with the same duration. It is clear that even for time-dependent noise, pulses derived from Eq. (4) outperform naive pulses over a wide range of noise strengths if the noise is sufficiently slow. Further details regarding the numerical simulation can be found in Appendix A.

The relationship between the evolution time and the distance along the curve has an additional geometrical interpretation: the plane curve can be viewed as a lightlike (or null) curve in 3D Minkowski space. This fact can be seen by rewriting Eq. (7) as  $-dt^2 + dx^2 + dy^2 = 0$ , which is the infinitesimal proper distance along a lightlike curve. In this interpretation, any  $\Omega(t)$  which cancels the first-order error maps onto a lightlike curve which starts and ends at the origin of 3D Minkowski space. Such a curve is necessarily confined within a lightcone with apex at  $x = y = t = 0$ , as shown in Fig. 4. This lightcone is a reflection of the quantum speed limit, which refers to the minimum time it takes to evolve from one quantum state to another [44, 48–51]. For a two-level

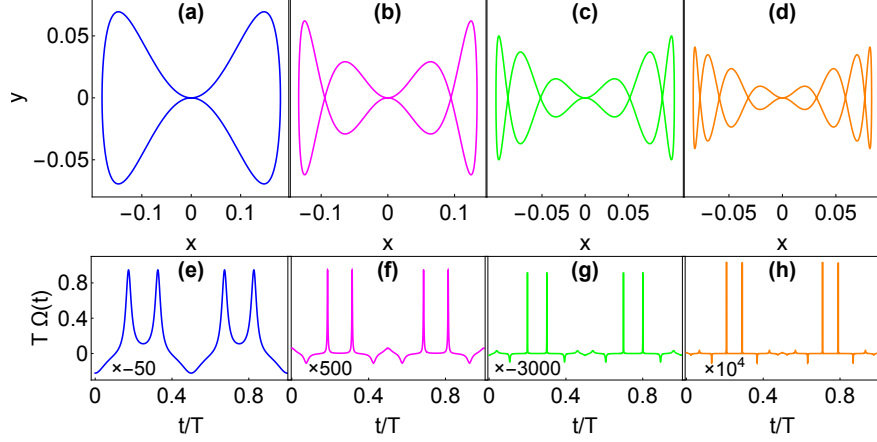


FIG. 5. Higher-order dynamical decoupling. (a-d) Plane curves from Eq. (18) with  $m = 2, 4, 6, 8$ . All curves have been rescaled to have unit length. (e-h) Corresponding pulses which implement identity operations while canceling up to first-, third-, fifth-, and seventh-order errors, respectively.

system, the quantum speed limit is saturated for zero driving,  $\Omega(t) = 0$ , which corresponds to a straight line in the plane, or equivalently a lightlike curve lying on the 3D lightcone. This is consistent with our earlier observation that  $\delta$ -function pulse sequences correspond to line segments in the plane: in the 3D Minkowski picture, the evolution between  $\delta$ -pulses is represented by lightlike curves (straight lines parallel to the lightcone), with a sharp bend for each pulse. This is illustrated in Fig. 4 for the case of spin echo.

The higher-order error-cancellation constraints give further restrictions on the shape of the plane curves. In Appendix B, we show that the constraints at arbitrary order  $n$  are built from two basic classes of integrals:

$$p_k(\lambda) = \int_0^\lambda d\mu r^k \theta', \quad q_k(\lambda) = \int_0^\lambda d\mu r^k \theta' e^{i\theta}, \quad (17)$$

where  $r$  and  $\theta$  are plane polar coordinates:  $re^{i\theta} = x + iy$ , and  $k$  is an integer. For example, third-order cancellation introduces the new constraint,  $q_3(\Lambda) = 0$ , while for fourth-order cancellation, we need  $p_4(\Lambda) = 0$ . These can be understood as requiring that certain signed volumes bounded by the plane curves must vanish. Consider for instance the constraint  $p_k(\Lambda) = 0$ . Since the area enclosed by the plane curve can be written as  $\int_0^\Lambda d\mu r^2(\mu) \theta'(\mu)$ , we recognize that  $p_k(\Lambda)$  is the volume lying between the plane curve area and the function  $F(r) = r^{k-2}$  over the plane. The constraints  $q_k(\Lambda) = 0$  admit a similar interpretation. In Appendix C, we show that the following family of deformed Geronno lemniscates parametrized by even integer  $m$ ,

$$x(\lambda) = \sin \lambda, \quad y(\lambda) = \frac{1}{2} \sin(m\lambda) \sin \lambda. \quad (18)$$

satisfy the error constraints up to order  $m - 1$ . These curves and their associated pulses are shown in Fig. 5,

where it is evident that higher-order errors are canceled by inserting additional self-intersections in the curve. These self-intersections allow integral constraints of the form  $p_{2n}(T) = 0$  to be satisfied since the lobes of the curve on either side of the intersection then have areas of opposite sign. Each additional lobe that appears in Fig. 5(a-d) has precisely the area need to cancel  $p_{2n}(T)$  for all  $n < m/2$ . Integrals of the type  $q_{2n+1}(T)$  for  $n < m/2$  cancel due to the inversion symmetry of the curves (see Appendix C). It is apparent from Fig. 5 that for fixed pulse time, the pulses become sharply peaked as higher-order errors are canceled. This is a consequence of needing to insert more turns and self-intersections in the plane curves in order to cancel higher-order errors, and it suggests that an all-orders error cancellation can only be achieved with  $\delta$ -function pulses. This is consistent with a no-go theorem [35] stating that all-orders error cancellation is not possible with finite pulses implemented within a finite time.

In conclusion, we have developed a geometrical framework that yields all possible driving fields that suppress inhomogeneous dephasing or errors due to qubit energy splitting fluctuations. We have used this framework to construct several explicit examples of smooth driving fields that implement dynamically corrected gates up to second order or dynamical decoupling to arbitrary order. The simple way in which the pulse shape is encoded in this geometrical construction (as the curvature of the plane curves) makes it straightforward to find optimal pulses given a set of system-specific constraints, for example on amplitude, slope, or overall pulse duration. Our framework thus provides a general, powerful approach to improving the control of qubit systems.

### Appendix A: $1/f$ noise simulation

This appendix provides details regarding our time-dependent  $1/f$  noise simulations. We simulate  $1/f$  noise as a sum over many random telegraph noise (RTN) sources:

$$\delta\beta(t) = \sum_{i=0}^N w_i \eta_i(t), \quad (\text{A1})$$

where  $\eta_i(t)$  represents a stochastic noise fluctuation for a single RTN source,  $N+1$  is the total number of RTN sources, and  $w_i$  is a weight factor that we must determine. The above expansion implies that

$$\begin{aligned} \langle \delta\beta(t) \delta\beta(0) \rangle &= \sum_{i=0}^N \sum_{j=0}^N w_i w_j \langle \eta_i(t) \eta_j(0) \rangle \\ &= \sum_{i=0}^N \langle \eta_i(t) \eta_i(0) \rangle w_i^2 = \sum_{i=0}^N e^{-2|t|/\tau_i} w_i^2, \end{aligned} \quad (\text{A2})$$

where in the final step, we used that different RTN sources are uncorrelated and that the two-point correlation function of the  $i$ th RTN source decays exponentially with characteristic timescale defined as  $\tau_i$ . Taking the Fourier transform of both sides, we find that the noise power spectrum is given by

$$S(\omega) = \sum_{i=0}^N \frac{4\tau_i}{4 + \omega^2 \tau_i^2} w_i^2. \quad (\text{A3})$$

We want to determine the RTN parameters such that this spectrum approximates that of  $1/f$  noise:

$$S(\omega) \approx \frac{A^2}{\omega}. \quad (\text{A4})$$

More precisely, this relation should hold in the continuum limit,  $N \rightarrow \infty$ . This will be the case if we choose the  $\tau_i$  to be equally spaced:

$$\tau_i = \frac{i}{N} (\tau_{\max} - \tau_{\min}) + \tau_{\min}, \quad (\text{A5})$$

and if we choose the weight factor to be

$$w_i^2 = \frac{A^2}{N\pi} \frac{\tau_{\max} - \tau_{\min}}{\tau_i}. \quad (\text{A6})$$

Eqs. (A1), (A5), and (A6) are what we use to approximate  $1/f$  noise using an ensemble of RTN sources in numerical simulations. For the numerical results shown in the main text, we take  $N = 10^5$ ,  $\tau_{\min} = 44T$ ,  $\tau_{\max} = 441T$ , and vary  $A$  so that the time-averaged noise strength,  $\langle |\delta\beta(t)| \rangle$ , varies from 0 to  $9.2/T$ , averaging over 50 instances of the noise for each value. The square pulse used in the comparison is taken to have the same duration,  $T$ , as our smooth error-correcting pulse, as well as the same area of  $3\pi$ . We use the definition of fidelity given in [47].

### Appendix B: Form of higher-order constraints

Starting from the recursion relation, Eq. (4), and performing integrations by parts multiple times yields one of four expressions depending on the value of  $n \bmod 4$ :

$$\begin{aligned} g_n &= g_{n-1}^* g_1 - g_{n-2} g_2^* + \dots - g_{(n+2)/2} g_{(n-2)/2}^* \\ &\quad + \int dt g_{n/2}^* \dot{g}_{n/2}, \quad n = 4m + 2, \\ g_n &= g_{n-1}^* g_1 - g_{n-2} g_2^* + \dots + g_{(n+2)/2}^* g_{(n-2)/2} \\ &\quad - \int dt g_{n/2} \dot{g}_{n/2}^*, \quad n = 4m + 4, \\ g_n &= g_{n-1}^* g_1 - g_{n-2} g_2^* + \dots + g_{(n+3)/2}^* g_{(n-1)/2} \\ &\quad - \int dt g_{(n+1)/2} \dot{g}_{(n-1)/2}^*, \quad n = 4m + 1, \\ g_n &= g_{n-1}^* g_1 - g_{n-2} g_2^* + \dots - g_{(n+3)/2} g_{(n-1)/2}^* \\ &\quad + \int dt g_{(n+1)/2}^* \dot{g}_{(n-1)/2}, \quad n = 4m + 3, \end{aligned} \quad (\text{B1})$$

where  $m$  is a nonnegative integer. We see that if we assume  $g_k(T) = 0$  for  $k < n$ , then the constraint  $g_n(T) = 0$  reduces to a condition involving two lower-order error coefficients:

$$\begin{aligned} \int_0^T dt g_{n/2}^* \dot{g}_{n/2} &= 0, \quad n \text{ even}, \\ \int_0^T dt g_{(n+1)/2}^* \dot{g}_{(n-1)/2} &= 0, \quad n \text{ odd}. \end{aligned} \quad (\text{B2})$$

Taking  $n = 2$  and working with plane polar coordinates,  $g_1 = r e^{i\theta}$ , we obtain

$$g_2(t) = \int_0^t d\tau g_1^* \dot{g}_1 = \frac{1}{2} r(t)^2 + i \int_0^t d\tau r^2 \dot{\theta}. \quad (\text{B3})$$

We recognize the integral on the right as the area enclosed by the plane curve when  $t = T$ . Using this result for  $g_2$  in Eq. (B2) and assuming  $r(T) = 0$ , we find that the third-order constraint simplifies to

$$g_3(T) = \frac{4i}{3} \int_0^T d\tau r^3 e^{i\theta} \dot{\theta} = 0. \quad (\text{B4})$$

Similarly, if we also assume  $g_2(T) = 0$ , then cancellation of the fourth-order constraint requires

$$g_4(T) = i \int_0^T d\tau r^4 \dot{\theta} = 0, \quad (\text{B5})$$

while for fifth order we have

$$g_5(T) = \frac{8i}{15} \int_0^T d\tau r^5 e^{i\theta} \dot{\theta} - \frac{8}{3} \int_0^T d\tau r^2 \dot{\theta} \int_0^t dt' r^3 e^{i\theta} \dot{\theta}, \quad (\text{B6})$$

and for sixth order,

$$g_6(T) = \frac{2i}{9} \int_0^T d\tau r^6 \dot{\theta} + \frac{16}{9} \int_0^T d\tau r^3 e^{i\theta} \dot{\theta} \int_0^t dt' r^3 e^{-i\theta} \dot{\theta}. \quad (\text{B7})$$

Notice that  $g_4(T)$  and  $g_6(T)$  are both purely imaginary (the latter assumes  $g_3(T) = 0$ ) as expected from Eq. (5). The fact that all these constraints consist of integrals of  $\dot{p}_k(t)$ ,  $\dot{q}_k(t)$  (which are defined in Eq. (17)) and their complex conjugates arises because the functions  $g_n(t)$  are themselves comprised of such terms. This in turn can be proven using induction in conjunction with Eq. (4).

### Appendix C: Dynamical decoupling to arbitrary order: Deformed Geroni lemniscates

In this appendix, we show that the deformed Geroni lemniscate of order  $m$  given in Eq. (18) solves the error-cancellation constraints up to order  $m-1$ . First, we show that integrals of the type  $p_{2n}(T/2)$  vanish for  $m > 2n$ , where  $p_k(t)$  is defined in Eq. (17). To do this, we begin by rewriting this integral:

$$\begin{aligned} p_{2n}(T/2) &\propto \int_0^\pi \sin^{2n}(\lambda) (\sin^2(m\lambda) + 4)^{n-1} d\sin(m\lambda) \\ &= \sum_{i=0}^{n-1} a_i \int_0^\pi \sin^{2n}(\lambda) \sin^{2i}(m\lambda) d\sin(m\lambda) \\ &= \sum_{i=0}^{n-1} \frac{a_i}{2i+1} \int_0^\pi \sin^{2n}(\lambda) d\sin^{2i+1}(m\lambda) \\ &= \sum_{i=0}^{n-1} \tilde{a}_i \int_0^\pi \sin^{2i+1}(m\lambda) \sin^{2n-1}(\lambda) \cos(\lambda) d\lambda \\ &= \sum_{i=0}^{n-1} \sum_{j=0}^i \tilde{a}_i b_j \int_0^\pi \sin((2j+1)m\lambda) \sin^{2n-1}(\lambda) \cos(\lambda) d\lambda. \end{aligned} \quad (C1)$$

In this formula, each term has the form

$$\begin{aligned} I_{2n+1} &= \int_0^\pi \sin(2\ell\lambda) \sin^{2n+1}(\lambda) \cos(\lambda) d\lambda \\ &= -\ell \int_0^\pi \cos(2\ell\lambda) \sin^{2n+2}(\lambda) d\lambda - n I_{2n+1}. \end{aligned} \quad (C2)$$

Thus we get  $I_{2n+1} = -\frac{\ell}{n+1} J_{2n+2}$ , where we have defined

$$J_{2n} = \int_0^\pi \cos(2\ell\lambda) \sin^{2n}(\lambda) d\lambda. \quad (C3)$$

Using integration by parts, we can also obtain

$$J_{2n+2} = \frac{-\ell}{n+1} I_{2n+1} + \frac{2n+1}{2n+2} J_{2n}, \quad (C4)$$

so we have in the end

$$I_{2n+1} = \frac{-(2n+1)\ell}{2(n+1+\ell)(n+1-\ell)} J_{2n}. \quad (C5)$$

We see from Eq. (C3) that  $J_0 = 0$ , so from the relation above it follows that for  $n+1 < \ell$  we have  $I_{2n+1} = 0$ . If we combine this conclusion with the formula in Eq. (C1), we find that as long as  $m > 2n$  the deformed Geroni lemniscate, Eq. (18), is able to cancel  $p_{2n}(T/2)$ . The cancellation of these integrals implies that  $p_{2n}(T)$  also vanishes.

The deformed Geroni lemniscates also cancel the integrals  $q_{2n+1}(T)$ , where  $q_k(t)$  is defined in Eq. (17). This follows from the curves' inversion symmetry. Every point,  $\lambda$ , along the curve has an inversion-related partner,  $\tilde{\lambda}$ , such that  $\theta(\tilde{\lambda}) = \pi + \theta(\lambda)$ ,  $r(\tilde{\lambda}) = r(\lambda)$ , and  $\theta'(\tilde{\lambda}) = \theta'(\lambda)$ . This implies that the contribution to  $q_{2n+1}(T)$  from the  $x < 0$  half of the curve exactly cancels that from the  $x > 0$  half.

In addition to terms like  $p_n(T)$  or  $q_n(T)$ , the  $n$ th order error coefficient also contains terms with nested integrals involving  $p_k(t)$  and  $q_k(t)$  (see e.g., Eqs. (B6) and (B7)). We do not have a proof that such terms also vanish identically for the deformed Geroni lemniscates, but we have verified this numerically up to seventh order and conjecture that this trend continues to arbitrary order.

- 
- [1] M. A. Nielsen and I. L. Chuang, *Quantum Computation and Quantum Information* (Cambridge University Press, Cambridge, England, 2000).
  - [2] D. Leibfried, R. Blatt, C. Monroe, and D. Wineland, *Rev. Mod. Phys.* **75**, 281 (2003).
  - [3] R. Hanson, L. P. Kouwenhoven, J. R. Petta, S. Tarucha, and L. M. K. Vandersypen, *Rev. Mod. Phys.* **79**, 1217 (2007).
  - [4] T. D. Ladd, F. Jelezko, R. Laflamme, Y. Nakamura, C. Monroe, and J. L. O'Brien, *Nature* **464**, 45 (2010).
  - [5] M. H. Devoret and R. J. Schoelkopf, *Science* **339**, 1169 (2013).
  - [6] N. Gisin, G. Ribordy, W. Tittel, and H. Zbinden, *Rev. Mod. Phys.* **74**, 145 (2002).
  - [7] N. Gisin and R. Thew, *Nat. Photon.* **1**, 165 (2007).
  - [8] J. J. Bollinger, W. M. Itano, D. J. Wineland, and D. J. Heinzen, *Phys. Rev. A* **54**, R4649 (1996).
  - [9] P. Maletinsky, S. Hong, M. S. Grinolds, B. Hausmann, M. D. Lukin, R. L. Walsworth, M. Loncar, and A. Yacoby, *Nat. Nanotechnol.* **7**, 320 (2012).
  - [10] C. L. Degen, F. Reinhard, and P. Cappellaro, *ArXiv e-prints* (2016), arXiv:1611.02427 [quant-ph].
  - [11] L. Chirrolli and G. Burkard, *Advances in Physics* **57**, 225 (2008).
  - [12] J. Bergli, Y. M. Galperin, and B. L. Altshuler, *New Journal of Physics* **11**, 025002 (2009).
  - [13] P. L. Stanwix, L. M. Pham, J. R. Maze, D. Le Sage, T. K. Yeung, P. Cappellaro, P. R. Hemmer, A. Yacoby, M. D. Lukin, and R. L. Walsworth, *Phys. Rev. B* **82**, 201201 (2010).
  - [14] J. M. Martinis and A. Megrant, *ArXiv e-prints* (2014), arXiv:1410.5793 [quant-ph].
  - [15] J. Koch, T. M. Yu, J. Gambetta, A. A. Houck, D. I. Schuster, J. Majer, A. Blais, M. H. Devoret, S. M. Girvin, and R. J. Schoelkopf, *Phys. Rev. A* **76**, 042319 (2007).
  - [16] M. Veldhorst, J. Hwang, C. Yang, A. Leenstra,



- B. de Ronde, J. Dehollain, J. Muhonen, F. Hudson, K. Itoh, A. Morello, and A. Dzurak, *Nat. Nanotechnol.* **9**, 981 (2014).
- [17] J. T. Muhonen, J. P. Dehollain, A. Laucht, F. E. Hudson, T. Sekiguchi, K. M. Itoh, D. N. Jamieson, J. C. McCallum, A. S. Dzurak, and A. Morello, *Nat. Nanotechnol.* **9**, 986 (2014).
- [18] E. L. Hahn, *Phys. Rev.* **80**, 580 (1950).
- [19] H. Y. Carr and E. M. Purcell, *Phys. Rev.* **94**, 640 (1954).
- [20] S. Meiboom and D. Gill, *Rev. Sci. Instrum.* **29**, 688 (1958).
- [21] U. Haeberlen, *High Resolution NMR in Solids, Advances in Magnetic Resonance Series, Supplement 1* (Academic, New York, 1976).
- [22] S. Wimperis, *J. Magn. Reson. B* **109**, 221 (1994).
- [23] L. Viola and S. Lloyd, *Phys. Rev. A* **58**, 2733 (1998).
- [24] K. Khodjasteh and D. A. Lidar, *Phys. Rev. Lett.* **95**, 180501 (2005).
- [25] G. S. Uhrig, *Phys. Rev. Lett.* **98**, 100504 (2007).
- [26] J. T. Merrill and K. R. Brown, *Progress in compensating pulse sequences for quantum computation, in quantum information and computation for chemistry: Advances in chemical physics*, vol. 154 (ed. S. Kais), John Wiley & Sons, Inc. (2014).
- [27] H. Bluhm, S. Foletti, I. Neder, M. Rudner, D. Mahalu, V. Umansky, and A. Yacoby, *Nat. Phys.* **7**, 109 (2011).
- [28] E. Kawakami, T. Jullien, P. Scarlino, D. R. Ward, D. E. Savage, M. G. Lagally, V. V. Dobrovitski, M. Friesen, S. N. Coppersmith, M. A. Eriksson, and L. M. K. Vandersypen, *PNAS* **113**, 11738 (2016).
- [29] F. K. Malinowski, F. Martins, P. D. Nissen, E. Barnes, L. Cywiński, M. S. Rudner, S. Fallahi, G. C. Gardner, M. J. Manfra, C. M. Marcus, and F. Kuemmeth, *Nat. Nanotechnol.* **12**, 16 (2017).
- [30] G. Goelman, S. Vega, and D. B. Zax, *J. Magn. Reson.* **81**, 423 (1989).
- [31] K. Khodjasteh, D. A. Lidar, and L. Viola, *Phys. Rev. Lett.* **104**, 090501 (2010).
- [32] T. van der Sar, Z. H. Wang, M. S. Blok, H. Bernien, T. H. Taminiau, D. Toyli, D. A. Lidar, D. D. Awschalom, R. Hanson, and V. V. Dobrovitski, *Nature* **484**, 82 (2012).
- [33] C. Kabytayev, T. J. Green, K. Khodjasteh, M. J. Biercuk, L. Viola, and K. R. Brown, *Phys. Rev. A* **90**, 012316 (2014).
- [34] A. Soare, H. Ball, D. Hayes, J. Sastrawan, M. C. Jarratt, J. J. McLoughlin, X. Zhen, T. J. Green, and M. J. Biercuk, *Nat. Phys.* **10**, 825 (2014).
- [35] X. Wang, L. S. Bishop, J. P. Kestner, E. Barnes, K. Sun, and S. Das Sarma, *Nat. Commun.* **3**, 997 (2012).
- [36] J. P. Kestner, X. Wang, L. S. Bishop, E. Barnes, and S. Das Sarma, *Phys. Rev. Lett.* **110**, 140502 (2013).
- [37] X. Wang, L. S. Bishop, E. Barnes, J. P. Kestner, and S. Das Sarma, *Phys. Rev. A* **89**, 022310 (2014).
- [38] E. Barnes, X. Wang, and S. Das Sarma, *Sci. Rep.* **5**, 12685 (2015).
- [39] F. A. Calderon-Vargas and J. P. Kestner, *ArXiv e-prints* (2016), arXiv:1607.04638 [quant-ph].
- [40] L. Cywiński, R. M. Lutchyn, C. P. Nave, and S. Das Sarma, *Phys. Rev. B* **77**, 174509 (2008).
- [41] F. Martins, F. K. Malinowski, P. D. Nissen, E. Barnes, S. Fallahi, G. C. Gardner, M. J. Manfra, C. M. Marcus, and F. Kuemmeth, *Phys. Rev. Lett.* **116**, 116801 (2016).
- [42] E. Barnes, M. S. Rudner, F. Martins, F. K. Malinowski, C. M. Marcus, and F. Kuemmeth, *Phys. Rev. B* **93**, 121407 (2016).
- [43] E. Barnes and S. Das Sarma, *Phys. Rev. Lett.* **109**, 060401 (2012).
- [44] E. Barnes, *Phys. Rev. A* **88**, 013818 (2013).
- [45] J. Medford, L. Cywiński, C. Barthel, C. M. Marcus, M. P. Hanson, and A. C. Gossard, *Phys. Rev. Lett.* **108**, 086802 (2012).
- [46] O. E. Dial, M. D. Shulman, S. P. Harvey, H. Bluhm, V. Umansky, and A. Yacoby, *Phys. Rev. Lett.* **110**, 146804 (2013).
- [47] M. D. Bowdrey, D. K. L. Oi, A. J. Short, K. Banaszek, and J. A. Jones, *Phys. Lett. A* **294**, 258 (2002).
- [48] L. Mandelstam and I. Tamm, *J. Phys. (USSR)* **9**, 249 (1945).
- [49] K. Bhattacharyya, *J. Phys. A: Math. Gen.* **16**, 2993 (1983).
- [50] N. Margolus and L. B. Levitin, *Physica D* **120**, 188 (1998).
- [51] V. Giovannetti, S. Lloyd, and L. Maccone, *Phys. Rev. A* **67**, 052109 (2003).